Analyst

Accepted Manuscript

ROYAL SOCIETY OF CHEMISTRY

www.rsc.org/analyst

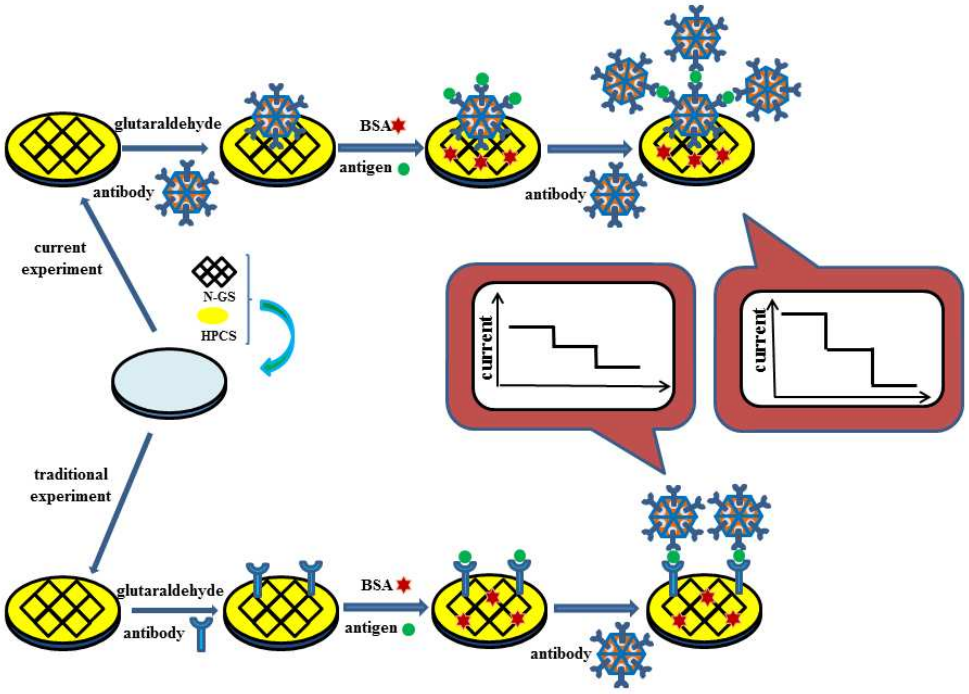

Ultrasensitive dual amplification sandwich immunosensor for breast cancer susceptibility gene based on sheet materials

Xiang Ren,[a] Tao Yan,[a] Sen Zhang,[b] Xiaoyue Zhang,[a] Picheng Gao,[a] Dan Wu,[a] Bin Du,[a,b] Qin Wei [a,*]

[a] Key Laboratory of Chemical Sensing & Analysis in Universities of Shandong, School of Chemistry and Chemical Engineering, University of Jinan, Jinan 250022, P.R. China

[b] School of Resources and Environmental Sciences, University of Jinan, Jinan 250022, PRChina

Correspondence: sdjndxwq@163.com (Qin Wei)

Tel: + 86-531-82767872

Fax: + 86-531-82765969

Abstract

A new electrochemical dual amplification sandwich immunosensor (DASI) for ultrasensitive and accurate detection of breast cancer susceptibility gene was designed based on the combination of N-doped graphene, hydroxypropyl chitosan and Co_3O_4 mesoporous nanosheet. N-doped graphene has better electroconductibility than traditional graphene. It is an ideal electrochemistry material with large specific surface area and little resistance. Hydroxypropyl chitosan replaces the pure chitosan in the immobilization of the sensor to realize the sensitivity increasement. Co_3O_4 mesoporous nanosheet can enhance the effective area of the immunoreaction. This kind of dual amplification sandwich immunosensor was first used to the detection of breast cancer susceptibility gene. It has a wide linear response range of 0.001-35 ng/mL and a low detection limit of 0.33 pg/mL. It demonstrated that the stability, selectivity and reproducibility of the sensor were acceptable. The fabricated immunosensor shows great potential application in early disease diagnosis.

1. Introduction

The earlier clinical diagnosis of tumor makers can be detected, the easier cancer can be cured successfully. Recently, the reliable and effective detection of tumor maker is current studies[1-3]. Breast cancer susceptibility gene (BRCA1), can be detected in the population of pancreatic cancer, stomach cancer and colon cancer[4]. BRCAl mutation, caused about 40%-50% of hereditary breast cancers, is closely combined with the occurrence of the family ovary and breast cancer[5]. Therefore it is extremely urgent for the high-risk to develop a new type method to detect the BRCAl tumor makers. Traditional ways in detecting BRCA1 include high performance liquid chromatography[6], enzymatic mutation detection[7] and protein truncation test[8]. However, these methods are complex and time-consuming, and the test processing requires large and expensive apparatus. Therefore, to develop a rapid, sensitive and cheap method for BRCA1 detection is a great challenge.

Electrochemical immunosensor is a kind of new method for the trace detection. It has been used in many fields such as food[9], molecular imprinting[10], tumor maker[11], virus analysis[12] and environmental estrogen analysis[13]. The sandwich immunosensor, compared with label-free or competitive type, exhibits a higher sensitivity and lower detection limit[11, 14, 15]. That may attribute to the fact that dual amplification sandwich immunosensor (DASI) can capture more antigens. In previous study,

sandwich immunosensor was used extensively due to its excellent payload capability like enzyme, metal ions or electron mediator[2]. But in this research, the DASI was fabricated by initial antibody and second antibody all incubated with mesoporous materials, thus leading to a dual amplification effect. The incubated initial antibody can capture more antigens to enhance the sensitivity, and the incubated second antibody which attached more noble metal nanoparticles can strengthen payload capability to amplify the reaction signals.

Graphene sheets (GS), a two-dimensional hexagonal lattice structure, has attracted a great deal of interest due to its high conductivity, large specific surface area, good biocompatibility and potential applications in immunosensors[16, 17]. Recently, N-doped graphene sheets (N-GS) have been used in many fields such as electrochemiluminescence, molecular imprinting, bettery and electrocatalysis[10, 18-20]. Typically, GS is a kind of good conductor, while the nitrogen replaces the carbon atom of the hexagonal lattice skeleton structure. Hence, the obtained N-GS exhibit excellent more electroconductibility than the GS. That can be explained as follows[20-22]: there exist six electrons outside of the carbon atom, and four in the six electrons are in four p orbital separately of the nuclear structure, so three of the four p orbital can be bonding each other due to the hexagonal lattice skeleton structure, which may lead to a hanging p orbital (one electron) unpaired. When the nitrogen replaces the carbon

atom of GS, there exist a p orbital with two electrons owing to the N has seven electrons and five of them are filled with four p orbital of the nuclear structure. According to the bond of hexagonal lattice skeleton structure of the GS, the remaining one is the two electrons p orbital, which can increase the amount of the unpaired electrons. And the electroconductibility of the GS derive from the electrons. In addition, such doped N atoms can decorate the graphene planar sheet and introduce a change in the Fermi level, engendering the doping effects and opening the band gap of the graphene. Therefore, the great electroconductibility of N-GS exceed GS.

Chitosan is widely used in immunosensors in view of its wonderful film-forming property[23]. Nowadays, many chitosan derivatives have been applied in electroanalytical chemistry[24]. Here, hydroxypropyl chitosan (HPCS), which is full of amino and can combine more biomolecule than chitosan, was used to fabricate the immunosensor. Mesoporous materials were used in immunosensors extensively, such as Fe_3O_4[25], SiO_2[26], mesoporous noble metal[27] and alloy[28, 29]. Many mesoporous materials are spherical or other block shapes with large specific surface area and abundant of pores and canals. However, a lot of pores and canals of the materials are inside of them, which may decrease the quantity of noble metal attached on the inner pores and block the reaction of immunizing conjugation. Therefore, mesoporous sheet materials are the perfect

candidate for the immunosensor. Here, mesoporous nano-Co_3O_4 sheet materials were synthesized for the DASI. The aminated Co_3O_4 is combined with silver nanoparticles to form the Ag@Co_3O_4. The initial antibody and second antibody are all incubated with it to the formation of Ab-Ag@Co_3O_4 because of the combination of Ag nanoparticles and amino.

Herein, a novel electrochemical DASI for the detection of BRCAl has been fabricated. The immune reaction based on the specific binding of antibody and antigen was performed on the sheet materials. N-GS can increase the electroconductibility significantly and decrease the protein resistance. Ag@Co_3O_4 can enlarge the effective specific surface area for the sensitive detection. This immunosensing method is novel and effective, which may provide a potential application in clinical tests.

Experimental section

Materials and reagents

Rabbit anti-BRCA1 (primary antibody), BRCA1 and BSA were purchased from Sigma-Aldrich. HPCS was gained from Lvshen Bioengineering Co., Ltd. (Nantong, China). Glutaraldehyde (25%), ammonia, sodium borohydride, silver nitrate, graphite, cobalt chloride hexahydrate and ethylene glycol were obtained from Sinopharm Chemical Reagent Co., Ltd. (Beijing, China). Phosphate buffer solutions (PBS) were prepared by compounding the solutions of KH_2PO_4 (0.067

mol/L) and Na_2HPO_4 (0.067 mol/L) to appropriate pH value. PBS was used as electrolyte for all electrochemistry measurements. Ultrapure water was used throughout the experiment. All other chemicals were of analytical reagents grade and used without further purification.

Apparatus

All electrochemical measurements were carried out on an electrochemical workstation (CHI760D, Chenhua Instrument Shanghai Co., Ltd., China). A conventional three-electrode configuration was used. Working electrode is glassy carbon electrode (GCE, 4 mm diameter); reference electrode is a saturated calomel electrode (SCE) and Pt as the counter electrode. Surface area measurements were performed on Micromeritics ASAP 2020 surface area and porosity analyzer (Quantachrome, United States). X-ray powder diffraction (XRD) patterns were acquired from a Bruker D8 Focus diffractometer (Germany) using CuKα radiation (40 kV, 30 mA) of wavelength 0.154 nm. Transmission electron microscope (TEM) images were recorded from a JEOL JEM-1400 microscope (Japan). Scanning electron microscope (SEM) and Energy Dispersive X-Ray Spectroscopy (EDS) were obtained by JEOL JSM-6700F microscope (Japan)

Synthesis of materials

The synthesis of N-GS can be devided into two steps: preparation of graphene oxide (GO) and process of doping nitrogen. GO was prepared

according to a reported method[30]. In detail, graphite powder (0.3 g) and potassium hypermanganate (1.8 g) were added into a solution of mixed acid (36 mL H_2SO_4 and 4 mL H_3PO_4). Then the mixture was kept stirring at 50 °C for 12 h. After that, the mixture was poured slowly onto a pre-prepared ice (~ 400 mL) and 6 mL H_2O_2 was added into it dropwise. Subsequently, the filtrate was centrifuged (8000 rpm, 30 min). The remaining solid was washed in succession with 200 mL of water, 200 mL of 30% HCl, and 200 mL of ethanol for 3 times. And the resulting solid was dried at vaccum at the temperature of 35 °C for 24 h. GO was synthesized successfully. N-GS was prepared simply based on GO[31]. The as-synthesized GO was firstly dispersed in DMF (0.5 mg/mL) under ultrasonically treatment for 30 min, and then heated in an oil bath (153 °C) for 1 h. The N-GS was synthesized successfully.

Mesoporous nano-Co_3O_4 was prepared as follows[32]. 10 mmol $CoCl_2 \cdot 6H_2O$ was dissolved into 50 mL ultrapure water to form a homogeneous solution under magnetic stirring. An appropriate amount of sodium hydroxide dissolved in 20 ml distilled water was dropwise into the above solution. The brown precipitation was centrifuged, washed with distilled water and absolute alcohol three times, and dried at 60 °C in vacuum for 12 h. Finally, the precipitation was heated at 400 °C for 1 h in the air and slowly cooled to room temperature. And the Co_3O_4 was obtained for further usage.

Ag nanoparticles (Ag NPs) were prepared by a classical approach[33]. Briefly, $AgNO_3$ (1 mL, 50 mM) and trisodium citrate (1 mL, 5% (w/w)) were mixed with ultrapure water under vigorous stirring for 1 h. Then 0.1 mM of $NaBH_4$ solid was added into above mixture. Under continuous stirring for about 20 min, the mixture's color changed to brown-yellow and indicated the successful synthesis of Ag NPs. Finally, the solution was continuously stirred until the color not change.

Aminated Co_3O_4 was synthesized from some reported methods[34, 35]. The as-synthetized Co_3O_4 (0.5 g) was dispersed in anhydrous toluene (50 mL) in a flask and heated to 70 °C. Then, 3-aminopropyltriethoxysilane (500 μL) was dropped to the solution rapidly and the reaction refluxed 3 h at constant temperature 70 °C. After centrifuged, the solid product was washed 3 times with absolute alcohol and dried at 30 °C for 24 h. A free-flowing powdery material was obtained. The aminated Co_3O_4 was shown to contain $-NH_2$ by ninhydrin test[36].

Ag@Co_3O_4 was prepared by mixing of Ag NPs and aminated Co_3O_4. Ag NPs can connect with $-NH_2$ tightly[37]. Thus, the aminated Co_3O_4 was put into Ag NPs solution and centrifuged to obtain Ag@Co_3O_4 until the supernate was a little yellow which indicated the Co_3O_4 adsorbed Ag NPs sufficiently.

Fabrication of the immunosensor

Scheme 1 illustrates the process of the proposed method. It can be

divided into two sections: incubation of the Ab-Ag@Co_3O_4 and fabrication of the immunosensor. From Scheme 1A, aminated Co_3O_4 is covered with Ag nanoparticles, and BRCAl antibodies can connect on it. From Scheme 1B, in current experiment, HPCS is mixed with N-GS under ultrasonication to form uniform solution and the 6 μL of the prepared solution (1.0 mg/mL) is dropped on the surface of the polished electrode. Then 6μL of the incubated Ab-Ag@Co_3O_4 is connected on it through glutaraldehyde and 3 μL of bovine serum albumin (BSA) is covered on the former layer to block the nonspecific active sites. Subsequently, BRCA1 antigens are adsorbed on the antibodies of Ab-Ag@Co_3O_4 through specific binding of the immune substance. Finally, 6 μL of the Ab-Ag@Co_3O_4 is dropped on the electrode. That is the preparation of the DASI. And the DASI achieve the effect of space amplification. In traditional method, the previous sandwich immunosensor is fabricated in a similar way[26, 38]. However, in the current research, the primary antibody was incubated with Ag@Co_3O_4 to amplify the antigen loading capacity instead of pure antibody. Therefore this kind is plane amplification. And in this way, the DASI (current experiment) can enhance the sensitivity than the common sandwich immunosensor (traditional experiment) due to the large amplification of the spatial effect.

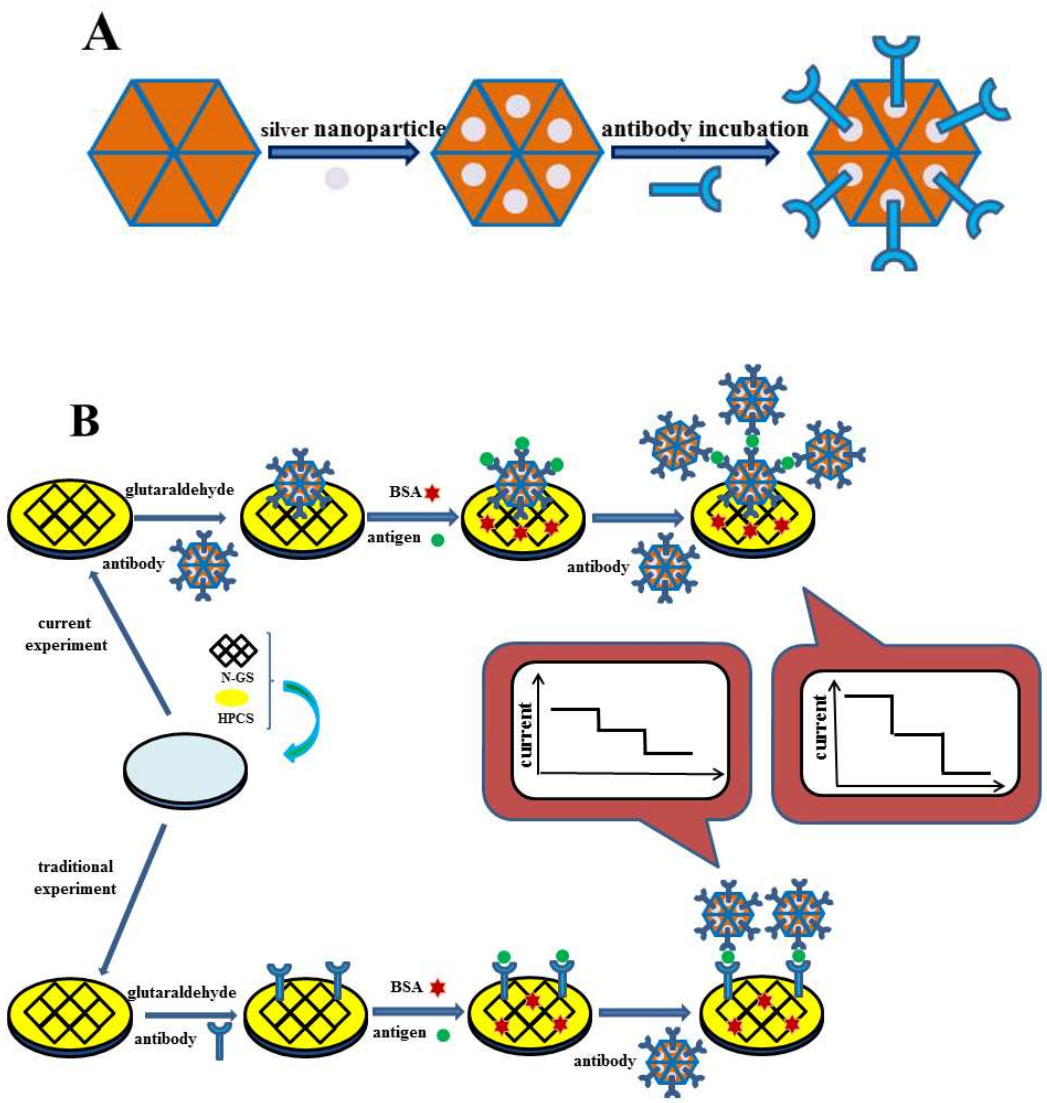

Scheme 1 the incubation of Ab-Ag@Co_3O_4 (A); fabrication of the DASI in both current experiment and traditional experiment (B)

Results and Discussion

Characterization of the materials

Fig. 1 shows the basic characterization of the N-GS. The base material of the sensor, exhibits the wrinkled paper morphology in the SEM image (Fig. 1A) and TEM image (Fig. 1B).

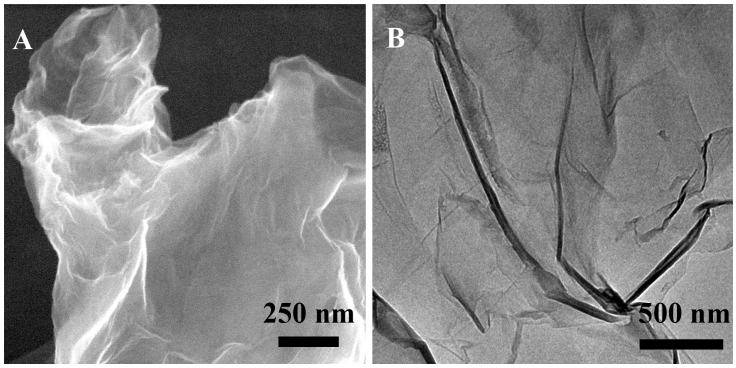

Fig. 1 SEM image (A) and TEM image (B) of N-GS

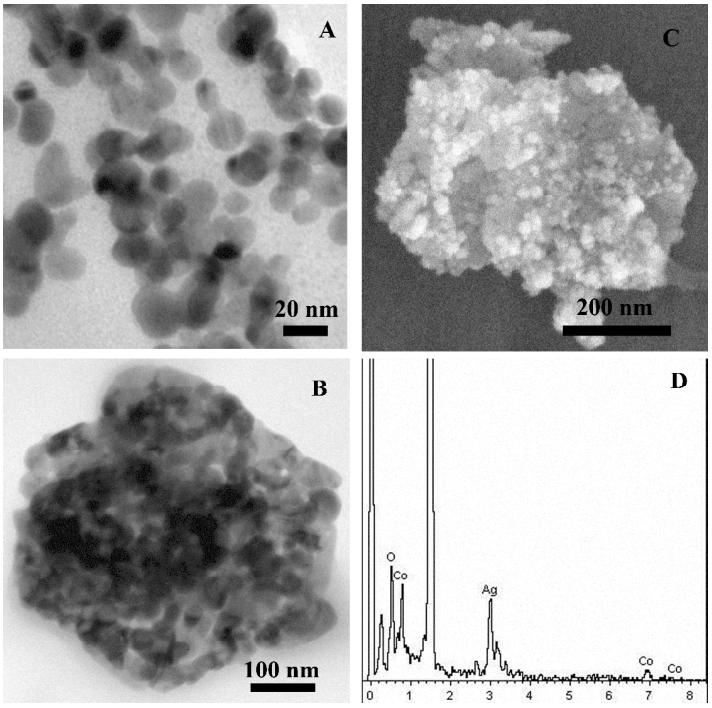

Fig. 2 TEM image (A) of Ag NPs, TEM image (D) of mesoporous Co_3O_4 nanosheet; SEM image (E) and EDS diagram (F) of the Ag@Co_3O_4.

From Fig. 2A, we can clearly observe the Ag NPs are about 15 nm in diameter. The mesoporous structure of the hexagon Co_3O_4 nanosheets can be seen from Fig. 2B, which demonstrates the holes of Co_3O_4 are irregular and without standard size. In this research, Ag@Co_3O_4 is used to prepare the sensor, and Ag@Co_3O_4 is also characterized by SEM (Fig. 2C)

and EDS (Fig. 2D). In Fig. 2C, there exists a mass of bright points attached on the surface and holes of hexagon. The bright points are the Ag nanoparticles combined on the aminated Co_3O_4. And EDS diagram further proves the Ag@Co_3O_4 synthesized successfully.

The morphology about the Co_3O_4 is detailed description above. But its specific information can be concluded from the XRD and BET (Fig. 3). The XRD patterns of cubic phase Co_3O_4 JCPDS card is No. 73-1701. And its diffraction pattern is in accordance with Fig. 3A. By Debye-Scherrer analysis, the lattice parameters a=b=c=8.08 Å accord with the standard values of cubic Co_3O_4. BET can reflect the specific information about the mesoporous nanosheet. Its BET surface area is 31.7745 m^2/g; pore volume (single point adsorption) is 0.1004 cm^3/g and the average pore size is 12.64 nm. In Fig. 3B, we can see cleary the adsorption line (the lower curve) and the desorption line (the upper curve) are nearly coincident, which demostrates the sheet material has much effect outside specific surface area.

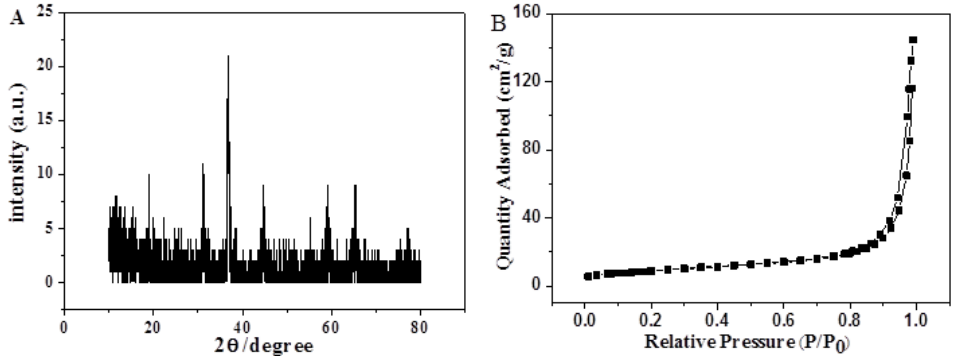

Fig. 3 XRD patterns of Co_3O_4 (A); BET analysis of Co_3O_4 (B)

Characterization of the immunosensor

To characterize the layer by layer self-assembly successfully, electrochemical impedance spectroscopy (EIS) was employed in the research using 2.5 mmol/L $Fe(CN)_6^{3-}/Fe(CN)_6^{4-}$ containing 0.1 mmol/L KCl solution. The EIS curves can be divided in two parts: the high frequency region and the low frequency region. The high frequency region is like a semicircle, which is related to the redox probe $Fe(CN)_6^{3-/4-}$. And the low frequency is a Warburg line corresponding to the diffusion step of overall process[39]. The resistance of the immunosensor can be calculated from the semicircle diameter in the nyquist plots of the EIS. In Fig. 4D, the nyquist plots of the EIS can be seen clearly. Curve a stands for the EIS of bare glassy carbon electrode (GCE) with a quite small semicircle diameter and a straight line, indicating the GCE polished well and held little resistance. Curve b represents the HPCS@N-GS modified layer, exhibiting a much small semicircle diameter than bare GCE that may be due to the N-GS super electroconductibility. Then the Ab-Ag@Co_3O_4 layer is described by curve c, which shows a big arc in high frequency because of the resistance of the BRCA1 antibody. Subsequently, BSA and BRCA1 antigen are dropped on the electrode, and their semicircle diameters of EIS plots (curve d and curve e) enhance gradually. Last, Ab-Ag@Co_3O_4 is connected again with a large diameter EIS plots. All the EIS plots indicate the layer by layer self-assembly was

effective.

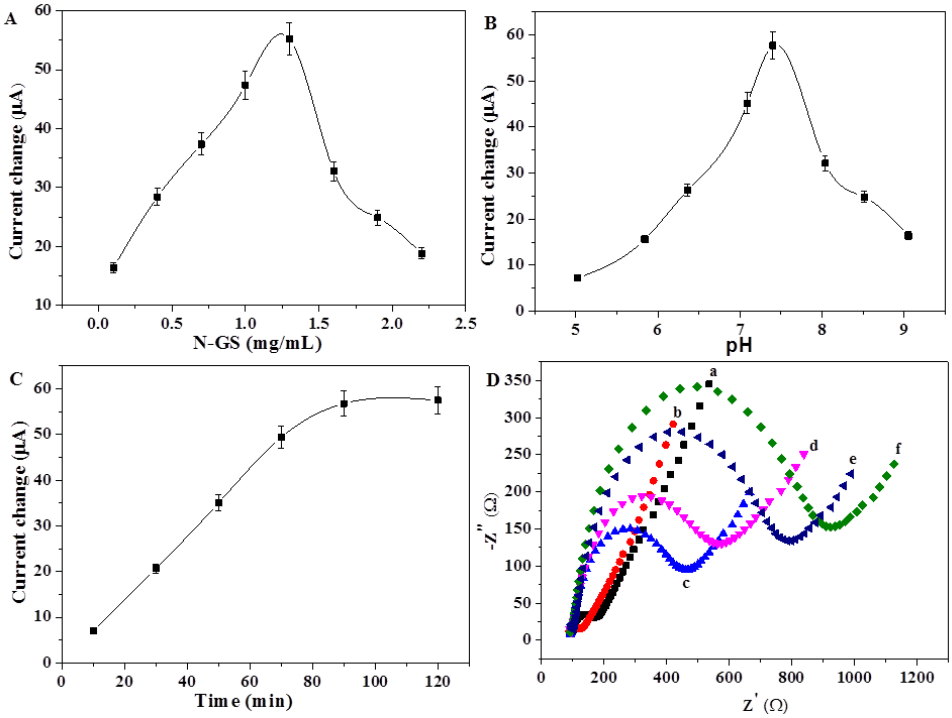

Fig. 4 A): effect of N-GS concentration on the response of the DASI (pH=7.4, BRCA1 antigen 20 ng/mL, *n*=5); B): effect of pH on the response of the DASI (N-GS 1.3 mg/mL, BRCA1 antigen 20 ng/mL, *n*=5); C): effect of incubation time on the response of the DASI (pH=7.4, N-GS 1.3 mg/mL, BRCA1 antigen 20 ng/mL, *n*=5); D): EIS obtained for different modified electrodes: (a) GCE, (b) GCE/HPCS@N-GS, (c) GCE/HPCS@N-GS/Ab-Ag@Co_3O_4, (d) GCE/HPCS@N-GS/Ab-Ag@Co_3O_4/BSA, (e) GCE/HPCS@N-GS/Ab-Ag@Co_3O_4/BSA/BRCA1, (f) GCE/HPCS@N-GS/Ab-Ag@Co_3O_4/BSA/BRCA1/ Ab-Ag@Co_3O_4.

Optimization of experimental conditions

In order to obtain the best analytical performance, some testing conditions have been optimized. N-GS are modified on the electrode to

amplify the area of the GCE without inducing great resistance. So the concentration of N-GS requires to be selected. In Fig. 4A, it is clear that the current change of the DASI firstly increases and then decreases, and the top point is 1.3 mg/mL. This phenomenon can be explained as follows: within low concentration, N-GS can increase the electroconductibility and enlarge contacting area, but in high concentration, N-GS electroconductibility cannot enough to offset overmuch layer resistance of the sheets. The best concentration is 1.3 mg/mL. The pH value is an important factor in the electrochemistry test as the acid-base condition may exhibit different results. In this research, pH=7.4 PBS (phosphate buffer solution) is selected as the best testing environment (Fig. 4B). That may be due to two reasons: First, neutral solution is suitable for the activity of biomolecule since the antibody-antigen linkage would be broken under alkalinity or acidity conditions; Second, in this research, H_2O_2 is selected as the signal source and $Ag@Co_3O_4$ exhibits obvious catalytic power to H_2O_2 in pH=7.4 PBS. Hence pH=7.4 PBS is chosen as the suitable buffer solution. Incubation time is also an important factor in the fabricating process. The incubation time can affect the loading quantity of the BRCA1 antigen and the activity of the biomolecule. From Fig. 4C, 90 min is selected as the adaptive incubation time with high signal response.

Analysis and detection

Under optimum testing conditions, the DASI was used to detect different concentrations of BRCA1 antigen. DASI was fabricated in Scheme 1 and H_2O_2 was used as the redox probe to record the electron transfer generated from H_2O_2 to the electrode when the immunological recation occurs. And the best potential to catalyze H_2O_2 was from -0.4 V to -0.2 V. The sensitivity of Ag@Co_3O_4 modified electrode toward H_2O_2 increased with the negative increase of detection potential. At higher detection potentials, such as -0.6 V, the background of the electrode is also increased and the O_2 reduction will interfere with H_2O_2 detection[40]. Thus, in this research, cyclic voltammograms were performed from -0.6 V to 0.2 V to show the electrochemical response and -0.4 V was selected the suitable reduction potential (Supplementary material, Fig. S1). After that, 5 mmol/L H_2O_2 was added into the buffer solution, and the current change was recorded (Supplementary material, Fig. S2). According to the current changes, calibration curve was drawn in Fig. 5. The current changed linely with logarithm of the antigen concentrations. The equation of the calibration curve is $Y = 41.43 + 11.39\ X$, r = 0.9978. And the linear range is 0.001-35 ng/mL with a low detection limit of 0.33 pg/mL at a signal to noise ratio of 3σ (where σ is the standard deviation of a blank solution, n = 11, r = 0.9978). And this method for the detection of BRCA1 has a better result than some reported researches (Table 1)[41-43]. The low detection limit can be attratubed to three factors: First, N-GS can

enhance the electroconductibility and specific surface area markedly; second, DASI can adsorb more antigens to amplify the signals or even in low antigen concentration, more signal source substance can connect on the only antigen; third, Co_3O_4 nanosheet can enlarge the effective contact area to magnify biological fixation loads.

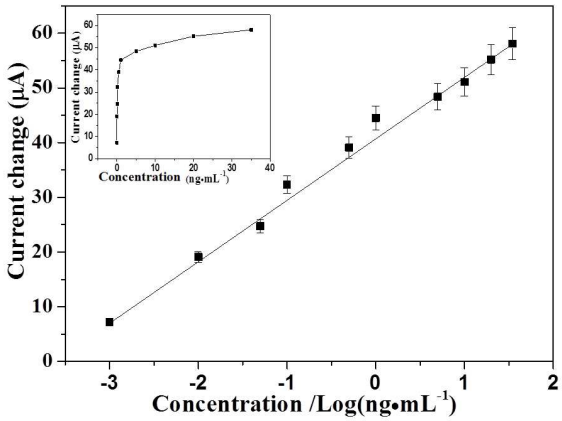

Fig. 5 Calibration curve of the prepared DASI towards different concentrations of BRCA1, error bar = RSD (n = 5).

scientific research	Linear range	Detection limit	Reference
Present research	0.001-35 ng/mL	0.33 pg/mL(10^{-15} mol/L)	
Biochip (molecular beacon detection scheme)	2×10^{-5}~5×10^{-6} mol/L	7×10^{-8} mol/L	41
Monolithic silicon optocoupler array	1×10^{-9}~5×10^{-7} mol/L	9×10^{-10} mol/L	42
Enzyme-free amplified detection platform	1×10^{-6}~1×10^{-13} mol/L	1×10^{-13} mol/L	43

Table 1 Comparison of the present research and other reports

Selectivity of DASI plays an essential role in the determination of analyzing biological samples[44]. Some else tumor makers were used to carry out the selectivity research. In Fig. 6, six DASIs were fabricated as the former way with 20 ng/mL of BRCA1, and five of them contain 200 ng/mL of different interfering antigens (alpha fetal protein, BSA, carcino-embryonic antigen, human immune globulin, melanoma antigen). The result displays that the current changes of the DASI were all less than 6.2% with adding interfering antigens which demonstrated the selectivity of DASI was acceptable. Stability is another factor of the DASI in potential practical application. Some fabricated electrodes were stored in refrigerator at 4 °C. 10 days later, the signal strength decreased to 98% of initial value. And one month later, compared with the initial, 95% signal strength was obtained. Reproducibility is also operated in this research. 5 prepared DASI were tested in identical conditions, and the relative standard deviation (RSD) of the measurement was 4.8%, suggesting the precision of the DASI was fairly good for the detection of BRCA1. The selectivity, stability and reproducibility of the DASI exhibit tiny current change, indicating the result was satisfactory and acceptable.

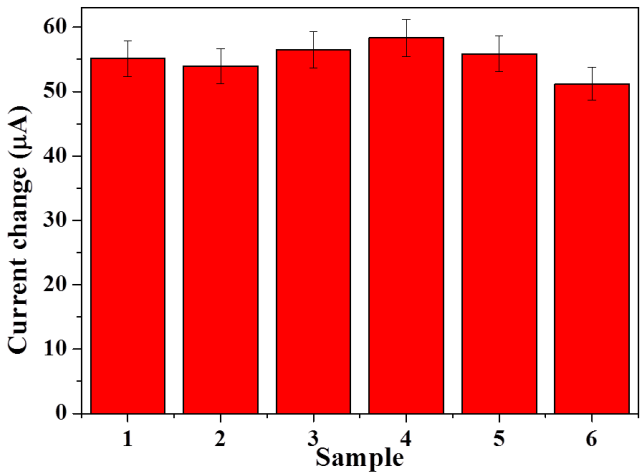

Fig. 6 The column of interference (1) 20 ng/mL BRCA1; (2) 20 ng/mL BRCA1+200 ng/mL alpha fetal protein; (2) 20 ng/mL BRCA1+200 ng/mL BSA, (3) 20 ng/mL BRCA1+200 ng/mL carcino-embryonic antigen; (4) 20 ng/mL BRCA1+200 ng/mL human immune globulin; (5) 20 ng/mL BRCA1+200 ng/mL melanoma antigen. Error bar=RSD (*n*=5).

Human serum sample (ng/mL)	The addition content (ng/mL)	The detection Content (ng/mL)	RSD (%, n=5)	Recovery (%)
0.83	1	1.81±0.04	1.60	101.8
0.83	5	5.86±0.07	5.41	100.5
0.83	10	10.92±0.08	6.95	100.9

Table 2 Results for the detection of BRCA1 in human serum sample by DASI.

In this research, in order to evaluate the performance of the sensor, human serum sample tests are carried out on DASI with standard addition method to verify the precision. The relative standard deviations (RSD) for

1 ng/mL, 5 ng/mL and 10 ng/mL are found to be 1.60%, 5.41%, 6.95%, respectively. And the achieved BRCA1 recoveries were 101.8%, 100.5% and 100.9%, respectively (Table 2).

Conclusion

In conclusion, we reported an Ag@Co_3O_4-based DASI for the sensitive detection of BRCA1. The strategy combines the advantages of N-GS and Ag@Co_3O_4 nanosheet. And HPCS was used in the sensor to enhance the biological adsorption. This novel immunosensor achieved a low detection limit of 0.33 pg/mL and a wide linear range of 0.001-35 ng/mL. This DASI had wonderful property of selectivity, stability and reproducibility, and human serum testing achieved a decent result. In addition, this DASI was easily manipulated and low cost. And the proposed method can test other tumor makers or it has potential application in clinical diagnosis.

Acknowledge

This study was supported by the Natural Science Foundation of China (No. 21175057, 21375047, 21377046), the Natural Science Foundation of Shandong Province (ZR2010ZR063), the Science and Technology Plan Project of Jinan (No. 201307010), and QW thanks the Special Foundation for Taishan Scholar Professorship of Shandong Province and UJN (No.ts20130937).

References

1. C. Zhang, D. Gao, G. Zhou, L. Chen, X. a. Zhang, Z. Cui and Z. He, *Asian J. Chem.*, 2012, **7**, 1764.
2. L.-N. Feng, Z.-P. Bian, J. Peng, F. Jiang, G.-H. Yang, Y.-D. Zhu, D. Yang, L.-P. Jiang and J.-J. Zhu, *Anal. Chem.*, 2012, **84**, 7810-7815.
3. A. Guo, D. Wu, H. Ma, Y. Zhang, H. Li, B. Du and Q. Wei, *J. Mater. Chem. B*, 2013, **1**, 4052-4058.
4. M. S. Brose, T. R. Rebbeck, K. A. Calzone, J. E. Stopfer, K. L. Nathanson and B. L. Weber, *J. Natl. Cancer Inst.*, 2002, **94**, 1365-1372.
5. M. Jhanwar-Uniyal, *Front. Biosci.*, 2003, **8**, s1107-1117.
6. S. H. Han, K. R. Lee, D. G. Lee, B. Y. Kim, K. E. Lee and W. S. Chung, *Clin. Genet.*, 2006, **70**, 496-501.
7. I. L. Andrulis, H. Anton‐Culver, J. Beck, B. Bove, J. Boyd, S. Buys, A. K. Godwin, J. L. Hopper, F. Li and S. L. Neuhausen, *Hum. mutat.*, 2002, **20**, 65-73.
8. N. van der Stoep, C. D. van Paridon, T. Janssens, P. Krenkova, A. Stambergova, M. Macek, G. Matthijs and E. Bakker, *Hum. mutat.*, 2009, **30**, 899-909.
9. Q. Wei, Y. Zhao, B. Du, D. Wu, H. Li and M. Yang, *Food Chem.*, 2012, **134**, 1601-1606.
10. X. Xue, Q. Wei, D. Wu, H. Li, Y. Zhang, R. Feng and B. Du, *Electrochim. Acta*, 2014, **116**, 366-371.
11. B. Jeong, R. Akter, O. H. Han, C. K. Rhee and M. A. Rahman, *Anal. Chem.*, 2013, **85**, 1784-1791.
12. C.-H. Zhou, Y. Shu, Z.-Y. Hong, D.-W. Pang and Z.-L. Zhang, *Asian J. Chem.*, **2013**, **8**, 2220-2226.
13. R. Feng, Y. Zhang, H. Yu, D. Wu, H. Ma, B. Zhu, C. Xu, H. Li, B. Du and Q. Wei, *Biosens. Bioelectron.*, 2012, **42**, 367-372.
14. J. Han, Y. Zhuo, Y. Chai, Y. Xiang, R. Yuan, Y. Yuan and N. Liao, *Biosens. Bioelectron.*, 2013, **41**, 116-122.
15. H. Li, Q. Wei, G. Wang, M. Yang, F. Qu and Z. Qian, *Biosens. Bioelectron.* , 2011, **26**, 3044-3049.
16. Z. Ao, A. Hernández-Nieves, F. Peeters and S. Li, *Phys. Chem. Chem. Phys.*, 2012, **14**, 1463-1467.
17. S. Zhang, B. Du, H. Li, X. Xin, H. Ma, D. Wu, L. Yan and Q. Wei, *Biosens. Bioelectron.*, 2014, **52**, 225-231.
18. Z. Lin, M.-k. Song, Y. Ding, Y. Liu, M. Liu and C.-p. Wong, *Phys. Chem. Chem. Phys.*, 2012, **14**, 3381-3387.
19. Y. Xue, J. Liu, H. Chen, R. Wang, D. Li, J. Qu and L. Dai, *Angew. Chem., Int. Ed.*, 2012, **51**, 12124-12127.
20. Y. Wang, Y. Shao, D. W. Matson, J. Li and Y. Lin, *Acs Nano*, 2010, **4**, 1790-1798.
21. L. Liu, S. Ryu, M. R. Tomasik, E. Stolyarova, N. Jung, M. S. Hybertsen, M. L. Steigerwald, L. E. Brus and G. W. Flynn, *Nano lett.*, 2008, **8**, 1965-1970.
22. Z. Mou, X. Chen, Y. Du, X. Wang, P. Yang and S. Wang, *Appl. Surf. Sci.*, 2011,

258, 1704-1710.
23. R. Feng, Y. Zhang, H. Ma, D. Wu, H. Fan, H. Wang, H. Li, B. Du and Q. Wei, *Electrochim. Acta*, 2013, **97**, 105-111.
24. G. Yang, J. Cao, L. Li, R. K. Rana and J.-J. Zhu, *Carbon*, 2012, **51**, 124-133.
25. S. Yu, Q. Wei, B. Du, D. Wu, H. Li, L. Yan, H. Ma and Y. Zhang, *Biosens. Bioelectron.*, 2013, **48**, 224-229.
26. L. Chen, Z. Zhang, P. Zhang, X. Zhang and A. Fu, *Sens. Actuators, B*, 2011, **155**, 557-561.
27. Z. Cui, D. Wu, Y. Zhang, H. Ma, H. Li, B. Du, Q. Wei and H. Ju, *Anal. Chim. Acta*, 2014, **807**, 44-50.
28. Q. Wei, Y. Zhao, B. Du, D. Wu, Y. Cai, K. Mao, H. Li and C. Xu, *Adv. Funct. Mater.*, 2011, **21**, 4193-4198.
29. Q. Lang, L. Li, A. Liu and H. Qiu, *Asian J. Chem.*, 2012, **7**, 2746-2746.
30. D. C. Marcano, D. V. Kosynkin, J. M. Berlin, A. Sinitskii, Z. Sun, A. Slesarev, L. B. Alemany, W. Lu and J. M. Tour, *Acs Nano*, 2010, **4**, 4806-4814.
31. K. Ai, Y. Liu, L. Lu, X. Cheng and L. Huo, *J. Mater. Chem.*, 2011, **21**, 3365-3370.
32. L. Li, Y. Wang, Y. Wang, Y. Han, F. Qiu, G. Liu, C. Yan, D. Song, L. Jiao and H. Yuan, *J. Power Sources*, 2011, **196**, 10758-10761.
33. Y. Wang, S. J. Zhen, Y. Zhang, Y. F. Li and C. Z. Huang, *J. Phys. Chem. C*, 2011, **115**, 12815-12821.
34. J. Zhu and J. He, *ACS Appl. Mater. Interfaces*, 2012, **4**, 1770-1776.
35. S. Yang, X. Feng, S. Ivanovici and K. Müllen, *Angew. Chem. Int. Ed.*, 2010, **49**, 8408-8411.
36. P. J. Lamothe and P. G. McCormick, *Anal. Chem.*, 1973, **45**, 1906-1911.
37. S. Jang, P. Thirupathi, L. N. Neupane, J. Seong, H. Lee, W. I. Lee and K.-H. Lee, *Org. Lett.*, 2012, **14**, 4746-4749.
38. J. Lu, S. Liu, S. Ge, M. Yan, J. Yu and X. Hu, *Biosens. Bioelectron.*, 2012, **33**, 29-35.
39. M. A. Panagopoulou, D. V. Stergiou, I. G. Roussis and M. I. Prodromidis, *Anal. Chem.*, 2010, **82**, 8629-8636.
40. Q. Wei, Z. Xiang, J. He, G. Wang, H. Li, Z. Qian and M. Yang, *Biosens. Bioelectron.*, 2010, **26**, 627-631.
41. M. Culha, D. L. Stokes, G. D. Griffin and T. Vo-Dinh, *Biosens. Bioelectron.*, 2004, **19**, 1007-1012.
42. E. Mavrogiannopoulou, P. S. Petrou, S. E. Kakabakos and K. Misiakos, *Biosens. Bioelectron.*, 2009, **24**, 1341-1347.
43. S. Shimron, F. Wang, R. Orbach and I. Willner, *Anal. Chem.*, 2011, **84**, 1042-1048.
44. P. R. Perrotta, F. J. Arévalo, N. R. Vettorazzi, M. A. Zón and H. Fernández, *Sens. Actuators, B*, 2012, **162**, 327-333.

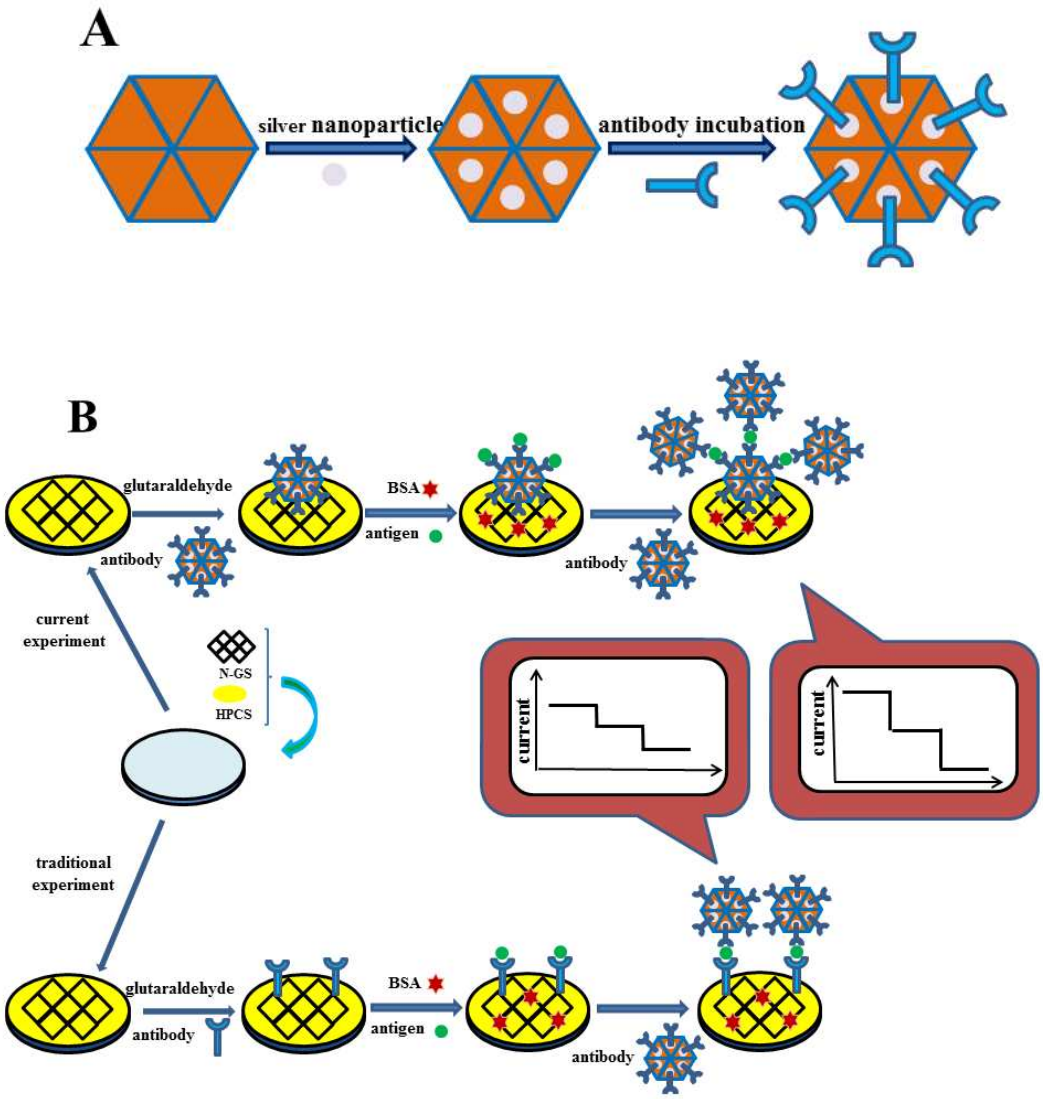

Scheme 1 the incubation of Ab-Ag@Co_3O_4 (A); fabrication of the DASI in both current experiment and traditional experiment (B)

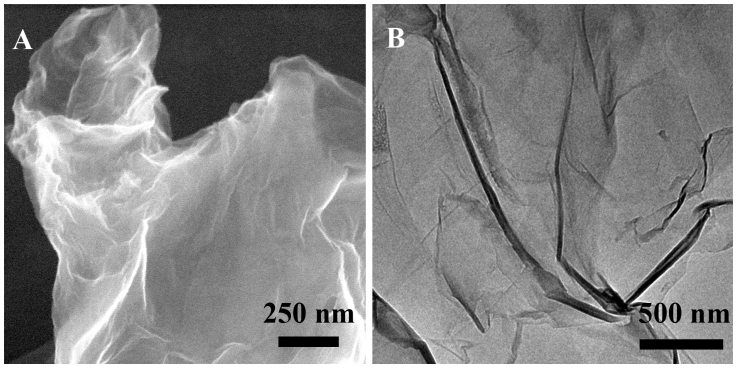

Fig. 1 SEM image (A) and TEM image (B) of N-GS

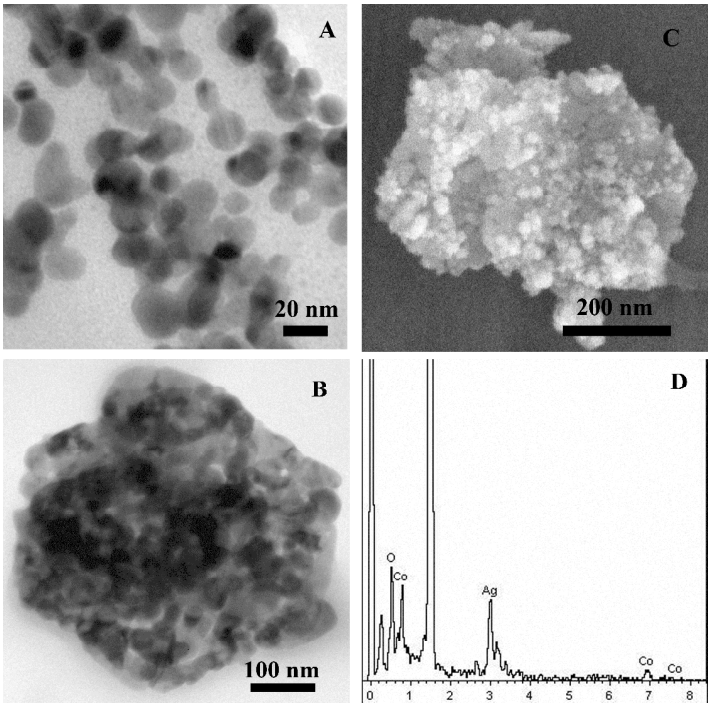

Fig. 2 TEM image (A) of Ag NPs, TEM image (D) of mesoporous Co_3O_4 nanosheet;

SEM image (E) and EDS diagram (F) of the Ag@Co_3O_4.

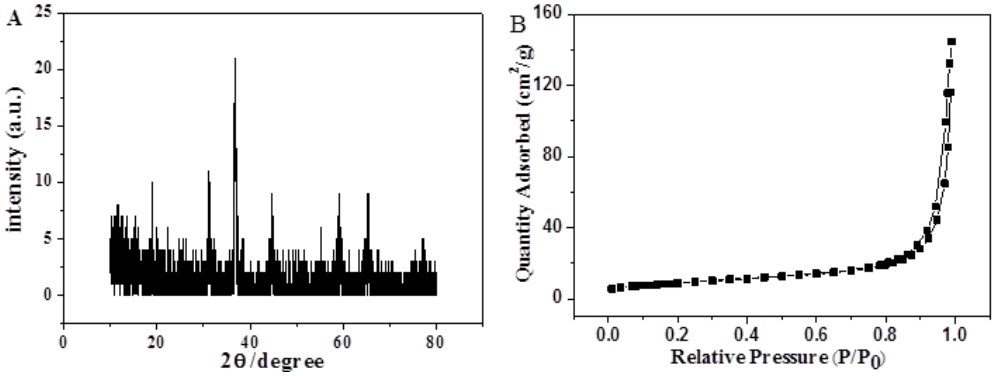

Fig. 3 XRD patterns of Co_3O_4 (A); BET analysis of Co_3O_4 (B)

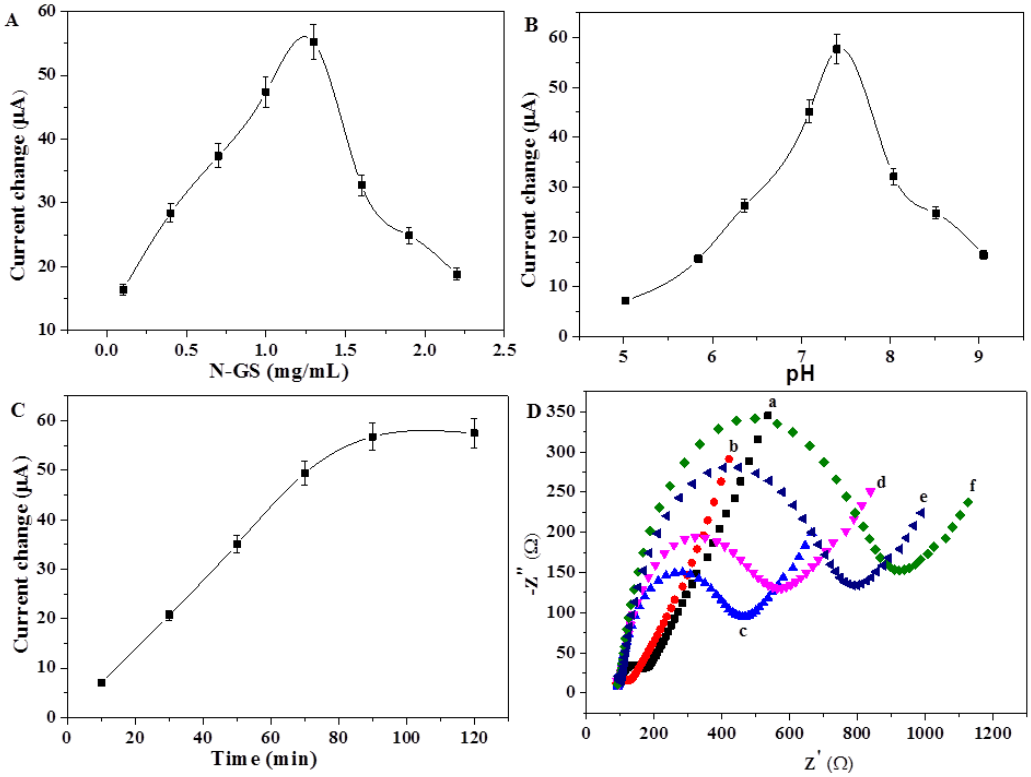

Fig. 4 A): effect of N-GS concentration on the response of the DASI (pH=7.4, BRCA1 antigen 20 ng/mL); B): effect of pH on the response of the DASI (N-GS 1.3 mg/mL, BRCA1 antigen 20 ng/mL); C): effect of incubation time on the response of

the DASI (pH=7.4, N-GS 1.3 mg/mL, BRCA1 antigen 20 ng/mL); D): EIS obtained for different modified electrodes: (a) GCE, (b) GCE/HPCS@N-GS, (c) GCE/HPCS@N-GS/Ab-Ag@Co_3O_4, (d) GCE/HPCS@N-GS/Ab-Ag@Co_3O_4/BSA, (e) GCE/HPCS@N-GS/Ab-Ag@Co_3O_4/BSA/BRCA1, (f) GCE/HPCS@N-GS/ Ab-Ag@Co_3O_4/BSA/BRCA1/ Ab-Ag@Co_3O_4.

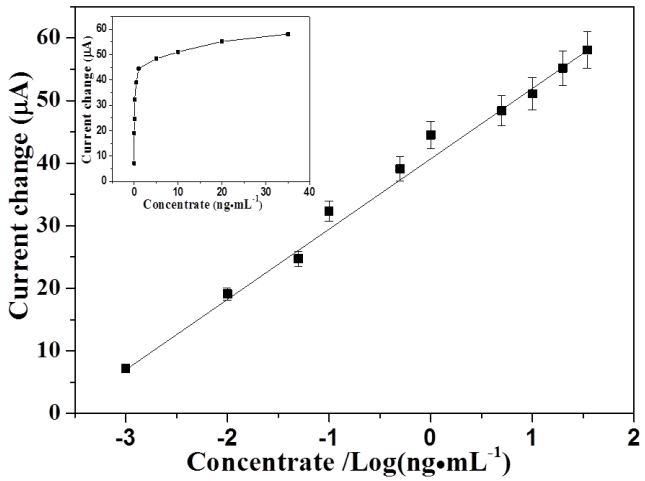

Fig. 5 Calibration curve of the prepared DASI towards different concentrations of BRCA1, error bar = RSD (n = 5).

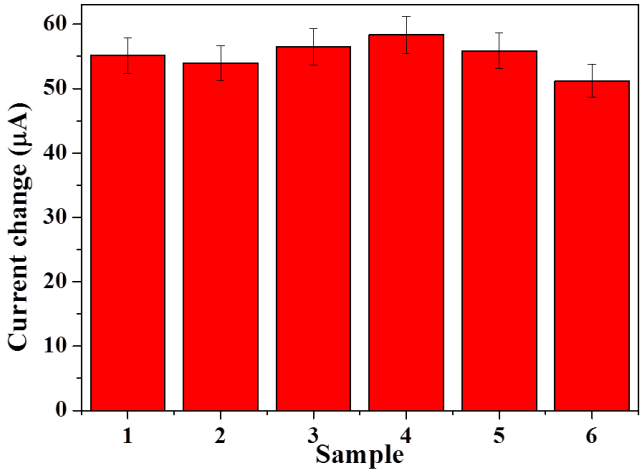

Fig. 6 The column of interference (1) 20 ng/mL BRCA1; (2) 20 ng/mL BRCA1+200 ng/mL alpha fetal protein; (2) 20 ng/mL BRCA1+200 ng/mL BSA, (3) 20 ng/mL BRCA1+200 ng/mL carcino-embryonic antigen; (4) 20 ng/mL BRCA1+200 ng/mL human immune globulin; (5) 20 ng/mL BRCA1+200 ng/mL melanoma antigen. Error bar=RSD (*n*=5).

scientific research	Linear range	Detection limit	Reference
Present research	0.001-35 ng/mL	0.33 pg/mL(10^{-15} mol/L)	
Biochip (molecular beacon detection scheme)	2×10^{-5}~5×10^{-6} mol/L	7×10^{-8} mol/L	41
monolithic silicon optocoupler array	1×10^{-9}~5×10^{-7} mol/L	9×10^{-10} mol/L	42
Enzyme-free amplified detection platform	1×10−6~1×10−13 mol/L	1 × 10−13 mol/L	43

Table 1 Comparison of the present research and other reports

Human serum sample (ng/mL)	The addition content (ng/mL)	The detection Content (ng/mL)	RSD (%, n=5)	Recovery (%)
0.83	1	1.81±0.04	1.60	101.8
0.83	5	5.86±0.07	5.41	100.5
0.83	10	10.92±0.08	6.95	100.9

Table 2 Results for the detection of BRCA1 in human serum sample by DASI.